Heterogeneous modelling behaviour at an interface in porous media

G. Quiroga-Goode * and J.M. Carcione

Osservatorio Geofisico Sperimentale, P.O. Box 2011, I-34016 Opicina, Trieste, Italy
E-mail: g.quiroga@ic.ac.uk

Received 12 September 1996

The fluid flow induced by an incident wave at a discontinuity separating two porous media is governed by the hydraulic permeabilities of both media and that of the interface. In the context of Biot's theory, we derive the time-harmonic Green's function for the two half-space problem allowing incident fast and slow dilatational waves to assess the heterogeneous modelling behaviour for diverse hydraulic conditions. It is found that when at least one of the media is permeated with inviscid fluids, heterogeneous modelling simulates open boundary conditions. On the other hand, when the model is saturated with viscous fluids, the modelling reproduces restrained fluid flow whose values correspond to sealed pore interface conditions, in agreement with the theoretical results. Therefore the numerical technique models correctly the wave diffusion and propagation phenomena attendant at the boundary.

Keywords: porous, boundary conditions, Green's function, heterogeneuos modelling

1. Introduction

The boundary conditions simulated by heterogeneous numerical modelling at physical interfaces are satisfied implicitly by the algorithm [11]. In this way, the solution of an additional set of equations expressing the continuity of the field variables across each interface is avoided. In models including a one-phase rheology, i.e., solids or fluids, where only one kind of boundary condition is satisfied, heterogeneous modelling has proved very useful, e.g., in studying AVO in anisotropic dissipative media [18], in using Love waves to locating coal seam discontinuities [12], in providing the forward solution for the inversion of seismic data [14], etc. However, in models involving boundaries separating two-phase media where interfacial flow can vary depending upon the hydraulic conditions of both media and that of the interface, it is not clear whether heterogeneous modelling simulates implicitly the correct wave diffusion and propagation phenomena.

Recent works have made use of heterogeneous schemes to study the seismic reponses from oil-saturated porous reservoirs [6,20]. However, no report is given on

* Present address: Imperial College, Department of Geology, London SW7 2BP, England.

an evaluation of the numerical approach by comparison with known analytical solutions for simpler geometries [3,7], mainly because no theoretical or experimental work is found in the literature describing the interface permeability as a function of porosities and pore fluid mobilities of the media.

A set of conditions were derived [8] sufficient for uniqueness of solution of the field equations whithin the context of Biot's theory of liquid-filled porous media. They represent different hydraulic conditions at interfaces leading to three different types of boundary equations (appendix B). Unrestrained fluid flow across the interface corresponds to an open boundary condition (OBC). In the case of a closed interface, the pores are sealed so that no fluid flow is produced through it, thus giving a closed boundary condition (CBC). In the intermediate case (MBC) there is a reduced interfacial flow, so that the boundary equations are parametrized by a surface impedance k, also called surface stiffness (or coefficient of resistance) that controls the amount of fluid transfer. This is the most representative situation for real problems. In the limiting cases where the surface impedance is zero or infinity, the boundary equations representing MBC reduce automatically to OBC and CBC, respectively.

From the theoretical formulation of the boundary conditions described above, it is clear that having high pore interconnectivity, meaning high interface permeability, implies efficient energy conversion into slow wave phenomena, although it is evident that the amplitudes of the converted modes must depend also on the hydraulic permeabilities of both media. Therefore, the significance of interface hydraulic permeability is greater than that indicated by other researchers [8] in which k was related solely to the degree of pore alignment. The choice of k is a delicate issue nevertheless and so far all problems have dealt with the limiting cases ($k = 0$ and $k = \infty$) [9,17,19]. In addition, the definition of k presupposes the interface to have finite length [2], whereas in naturally occurring porous materials, it has no thickness.

Ideally, the interface permeability should be an implicit parameter for a given set of physical properties of both media, assuming a random alignment of the pores on both sides of the interface. This seems to be the case of heterogeneous numerical modelling, as will be seen below.

To investigate the problem of heterogeneous modelling behaviour at an interface, we consider Biot's theory in the low-frequency range [1], and reflection and transmission for normal incidence for the most general case of incident fast and slow compressional waves including the three types of boundary conditions. Then we compare the analytical and the numerical solutions in order to assess whether the heterogeneous numerical scheme simulates the proper boundary conditions.

This work is divided in the following manner: The field equations for a 1D homogeneous unbounded medium are presented in section 2. Section 3 presents the Green's functions for two homogeneous porous media in contact involving the different types of boundary conditions. Then, in section 4 a brief description of the numerical methods is given. The results are presented in section 5 where the numerical solution of Biot's equations are compared with the analytical results for different fluid viscosities. The effect of modifying the viscosities in the model is to produce a change of the

hydraulic conditions of the interface, from OBC to MBC and to CBC which will alter the amplitudes of all scattered waves. The conclusions are given in section 6.

2. Field equations

The dynamic equations describing wave propagation in heterogeneous porous media are given by Biot [1]. For a compressional source, the problem of normal incidence prevents the existence of shear energy by mode conversion at discontinuities. In this way, the original Biot's equations can be simplified to model only dilatational deformations, i.e., fast and slow compressional waves. This is accomplished by taking the solid rigidity equal to zero. The 1D velocity-pressure formulation of Biot's *poro-acoustic* equations in the low frequency range, in the x-direction, is

$$\partial_t v = \beta_{11}\partial_x p + \beta_{12}\partial_x p_f + \frac{\eta}{\kappa}\beta_{12} q, \tag{1}$$

$$\partial_t q = -\beta_{21}\partial_x p - \beta_{22}\partial_x p_f - \frac{\eta}{\kappa}\beta_{22} q, \tag{2}$$

$$\partial_t p = -H\partial_x v - C\partial_x q + \dot{s}, \tag{3}$$

$$\partial_t p_f = -C\partial_x v - M\partial_x q + \dot{s}_f, \tag{4}$$

where v and q are the solid and relative fluid (filtration velocity) particle velocities, p is the bulk hydrostatic stress, and p_f is the fluid pressure, respectively. Here,

$$H = \left[{K_m}^{-1} - {K_s}^{-1} - \phi\left({K_s}^{-1} - {K_f}^{-1}\right)\right]K^{-1}, \tag{5}$$

$$C = \left({K_m}^{-1} - {K_s}^{-1}\right)K^{-1}, \tag{6}$$

$$M = {K_m}^{-1}K^{-1}, \tag{7}$$

with

$$K = \phi {K_m}^{-1}\left({K_f}^{-1} - {K_s}^{-1}\right) + {K_s}^{-1}\left({K_m}^{-1} - {K_s}^{-1}\right), \tag{8}$$

where K_s, K_m and K_f are the bulk moduli of the solid, matrix and fluid, respectively, and ϕ is the effective porosity. Moreover, η is the dynamic fluid viscosity and κ is the global permeability. Finally,

$$\boldsymbol{B} \equiv \begin{bmatrix} \beta_{11} & \beta_{12} \\ \beta_{21} & \beta_{22} \end{bmatrix} = \left({\rho_f}^2 - \rho m\right)^{-1} \begin{bmatrix} m & -\rho_f \\ \rho_f & -\rho \end{bmatrix}, \tag{9}$$

where $\rho = (1-\phi)\rho_s + \phi\rho_f$ is the composite density, with ρ_s and ρ_f the solid and fluid densities, and $m = \alpha\rho_f/\phi$ with α the tortuosity, a dimensionless parameter that depends on the pore geometry.

The source terms s and s_f can be expressed as

$$\boldsymbol{S} \equiv (s, s_f)^T = (1, \xi)^T h(t)\delta(x + x_0),$$

where $h(t)$ is the time history, $-x_0$ is the location ($x_0 > 0$) and δ denotes the delta function. In [5], three cases are considered:

- Bulk source: here it is assumed that the energy is partitioned between the two phases. In this case, $\xi = 1$.
- Solid source: $\xi = 0$.
- Fluid volume injection: $\xi = \phi^{-1}$.

3. Green's function for two media in contact

Let us consider two mono-dimensional porous media in contact at $x = 0$ and assume that fast and slow compressional waves, generated at $x = -x_0$, impinge upon the interface. The Green's function can be expressed as a linear combination of the fast and slow incident and scattered waves. The unit-impulse response corresponding to the solid particle velocity is

$$\begin{aligned} G_v(x,\omega) = \big\{ &\exp\big[\mathrm{i}\omega(x+x_0)/V_1\big] + \gamma_s \exp\big[\mathrm{i}\omega(x+x_0)/V_2\big] \\ &+ (R_{11}+R_{21})\exp(-\mathrm{i}\omega x/V_1) + (R_{12}+R_{22})\exp(-\mathrm{i}\omega x/V_2)\big\} H(-x) \\ &+ \big\{(T_{11}+T_{21})\exp\big(-\mathrm{i}\omega x/V_1'\big) \\ &+ (T_{12}+T_{22})\exp\big(-\mathrm{i}\omega x/V_2'\big)\big\} H(x), \end{aligned} \tag{10}$$

where H is the step function. γ_s gives the relative amplitude between the fast and slow waves supported by the medium and $V_{1,2}$ are their corresponding velocities. They are obtained in appendix A for a homogeneous unbounded medium. R_{ij} and T_{ij}, $i,j = 1,2$, are the relative particle velocity reflection and transmission coefficients, respectively. They are obtained in appendix B by solving the appropriate boundary conditions. Since the media are porous, they depend on the hydraulic conditions of the interface, thus the surface impedance k must be specified. The first subindex indicates the type of incident wave and the second the type of scattered wave, where 1 stands for fast wave and 2 for slow wave. Primed quantities correspond to those in the transmission medium.

The Green's function corresponding to the relative fluid particle velocity is

$$\begin{aligned} G_q(x,\omega) = \big\{ &\beta_1 \exp\big[\mathrm{i}\omega(x+x_0)/V_1\big] + \beta_1\gamma_f \exp\big[\mathrm{i}\omega(x+x_0)/V_2\big] \\ &+ \beta_1(R_{11}+R_{21})\exp(-\mathrm{i}\omega x/V_1) \\ &+ \beta_2(R_{12}+R_{22})\exp(-\mathrm{i}\omega x/V_2)\big\} H(-x) \\ &+ \big\{\beta_1'(T_{11}+T_{21})\exp\big(-\mathrm{i}\omega x/V_1'\big) \\ &+ \beta_2'(T_{12}+T_{22})\exp\big(-\mathrm{i}\omega x/V_2'\big)\big\} H(x), \end{aligned} \tag{11}$$

where

$$\gamma_f = \frac{\chi_2}{\chi_1} \tag{12}$$

gives the relative amplitude between the fast and slow waves in q. $\beta_{1,2}$, obtained in appendix A, correspond to the relative weights between the solid and relative fluid particle velocities for the fast (1) and slow (2) waves, respectively. The particle

velocities are obtained by multiplying the Green's function by the source spectrum and performing a Fourier transform (numerically) back to the time domain.

4. Numerical modelling

The goal of this work, as stated in the introduction, is to determine whether heterogeneous numerical modelling simulates implicitly the solution to the appropriate boundary equations depending on the hydraulic conditions of the interface separating two dissimilar porous media. We resort to two distinct explicit time-domain heterogeneous schemes. In this way it is possible to check that both numerical solutions reproduce exactly the same results.

The presence of diffusive modes in porous media makes Biot's differential equations *stiff* [10]. This condition practically precludes the use of standard explicit time integration techniques, since they require a very small time step to satisfy the stability condition.

The problems posed by the stiffness of the equations are circumvented by using a partition (or splitting) time integrator which allows for an efficient explicit solution [4] as in the case of non-stiff differential equations. The stiff system can be partitioned into two sets of differential equations, one stiff and the other nonstiff, such that they can be treated by two different methods, one implicit and the other explicit, respectively. The splitting technique yields the analytical solution of the stiff part, and the solution of the non-stiff part by a high-order scheme. The resulting algorithm, that we call scheme 1, possesses fourth-order accuracy in time and "infinite" (spectral) accuracy in space [13]. When the model is non-dissipative, i.e., viscosity $\eta = 0$, the usual stability conditions for acoustic wave propagation apply [20].

Alternatively, a staggered second-order algorithm [4], that we call scheme 2, based on a Crank–Nicolson method, with similar stability properties, although lower accuracy, is used to ascertain that heterogeneous modelling is independent of the numerical methods considered.

In the grid methods described above, the presence of discontinuities is represented naturally by spatial changes of the elastic constants H, C and M and/or the microstructural parameters (elements of $\boldsymbol{B}$, ϕ and η). The advantage of the numerical approach over the analytical one is that the surface impedance k of the interface is implicitly accounted for by the changes in porosities and/or the hydraulic permeabilities of both media.

5. Results

We consider an interface separating a brine saturated shale (incidence medium) and an oil saturated sandstone (transmission medium), whose material properties are given in table 1. It should be noted that although both media in the model have high porosities, which may imply that pore interconnectivity at the interface can be high,

the incidence medium posseses very low pore fluid mobility (κ/η) which may restrain the amount of flow at and from the boundary induced by the incident waves, as will be shown below.

As explained in the indroduction, the theoretical reflection and transmission coefficients (see appendix B) $R_{ij},\ T_{ij},\ i,j=1,2$, are dependent on the interface hydraulic conditions through k, the surface impedance factor that controls the amount of fluid transfer. It can obtained from (32)

$$k = \frac{p_f - p_f'}{q},$$

which is Darcy's law applied to the interface [8]. Its value is estimated directly from the field variables computed with the numerical modelling, i.e., it is the ratio of the pore fluid pressure drop in the two nodes adjacent to the interface and the filtration velocity in a grid point near the boundary. The primed variable corresponds to that in the transmission medium.

The low-frequency Biot theory is valid for frequencies less than $\eta\phi/(2\pi\alpha\kappa\rho_f)$, which for the media defined in table 1 are 1220 MHz and 7.95 MHz, respectively. The time-history of the source is

$$h(t) = \sin(\omega_0 t) - \frac{1}{2}\sin(2\omega_0 t), \quad 0 < t < \frac{2\pi}{\omega_0}, \tag{13}$$

where $\omega_0 = 2\pi f_0$, with $f_0 = 4.5$ kHz the central frequency. Its time Fourier transform is

$$\tilde{h}(\omega) = \frac{3\omega_0^3}{(\omega_0^2 - \omega^2)(4\omega_0^2 - \omega^2)}\left[\exp(2\pi \mathrm{i}\omega/\omega_0) - 1\right]. \tag{14}$$

In these experiments, a bulk source ($\xi = 1$ in equations (3) and (4)) of compressional waves is located at $x_0 = 70$ cm to the left of the interface. It excites four direct

Table 1
Material properties. 1 cp $= 10^{-3}$ Pa s; 1 mD $= 10^{-15}$ m^2.

Medium		Incidence (shale)	Transmission (sandstone)	
Solid	bulk modulus, K_s	7.6	40	GPa
	density, ρ_s	2210	2500	kg/m^3
Matrix	bulk modulus, K_m	6.17	20	GPa
	porosity, ϕ	0.16	0.2	
	permeability, κ	0.01	600	mD
	tortuosity, α	2	2	
Fluid	bulk modulus, K_f	2.5	1.85	GPa
	density, ρ_f	1040	880	kg/m^3
	viscosity, η	1	264	cp

waves: one fast and one slow travelling to the left (decreasing x, see appendix A) and another fast and another slow travelling towards the interface (increasing x).

In figures 1a–1d we compare analytical and numerical snapshots of the particle velocity field for a non-dissipative model, which corresponds to one permeated with inviscid fluids. The numerical solution was obtained with scheme 1 and cross-checked with the scheme 2 described above in this and all the other examples below. Since they produce exactly the same synthetics, we display only the results of one of them.

The coefficient of resistance k estimated from the numerical modelling and input for the theoretical reflection and transmission coefficients, was found to be negligible (22 N/m^3). This value corresponds to almost the OBC case, as can be observed in figures 1e and 1f where the analytic solid particle velocity reflection coefficients R_{11} and R_{12} are plotted as a function of the surface impedance k. In these plots, the scattering coefficients for the OBC and CBC cases correspond to the asymptotic values on the left and on the right respectively, whereas the MBC case represents the remaining ones. In practice, as the curve levels off rapidly towards the limiting OBC and CBC cases, the magnitude of the reflection coefficients overlaps with the MBC case for about two orders of magnitude on both sides with little appreciable change. As can be expected, decreasing the interface permeability, meaning that interfacial flow is being reduced, affects the amplitudes of all scattered waves such that the energy is being transferred from the slow waves to the fast waves. The other six scattering coefficients show similar behaviour.

As can be seen in figures 1a–1d, the numerical solution agrees very well, both in the solid (figure 1a) and in the relative fluid particle velocities (figure 1c), with its analytical counterpart. It simulates free fluid flow conditions across the interface, as expected, since both media in the model have infinite fluid mobility and high porosities. The snapshots were obtained at 1.85 ms and the interface is drawn with a vertical dotted line. All amplitudes in these and all the subsequent snapshots are normalized with respect to the largest amplitude. The amplitudes of q are approximately 1.2 larger than those of v. The direct P_1 travelling to the left is out of the range displayed.

In order to show the effects that a change of the type of boundary condition has on the seismic waveforms, already implied in figures 1e and 1f, figures 1b and 1d show the snapshots obtained by subtracting the analytical response for an OBC from that for a CBC. They are drawn to the same scale as plots 1a and 1c, respectively. As can be seen, most of the differences in amplitudes are related to the slow wave. The relative fluid particle velocity is more sensitive to changes in the hydraulic conditions of the interface, as can be observed in figure 1d, especially in the scattered waves generated by the slow incident mode. The converted fast waves (P_{21}) are also sensitive to changes in the type of boundary condition but only in the solid particle velocity v, as can be observed in figure 1b. In these plots (b and d), the direct slow wave P_2 travelling to the left has been cancelled as expected, since it is independent of the boundary conditions.

A slightly different picture can be observed in figure 2 where the transmission medium is permeated with oil, causing the pore fluid mobility to become finite. In

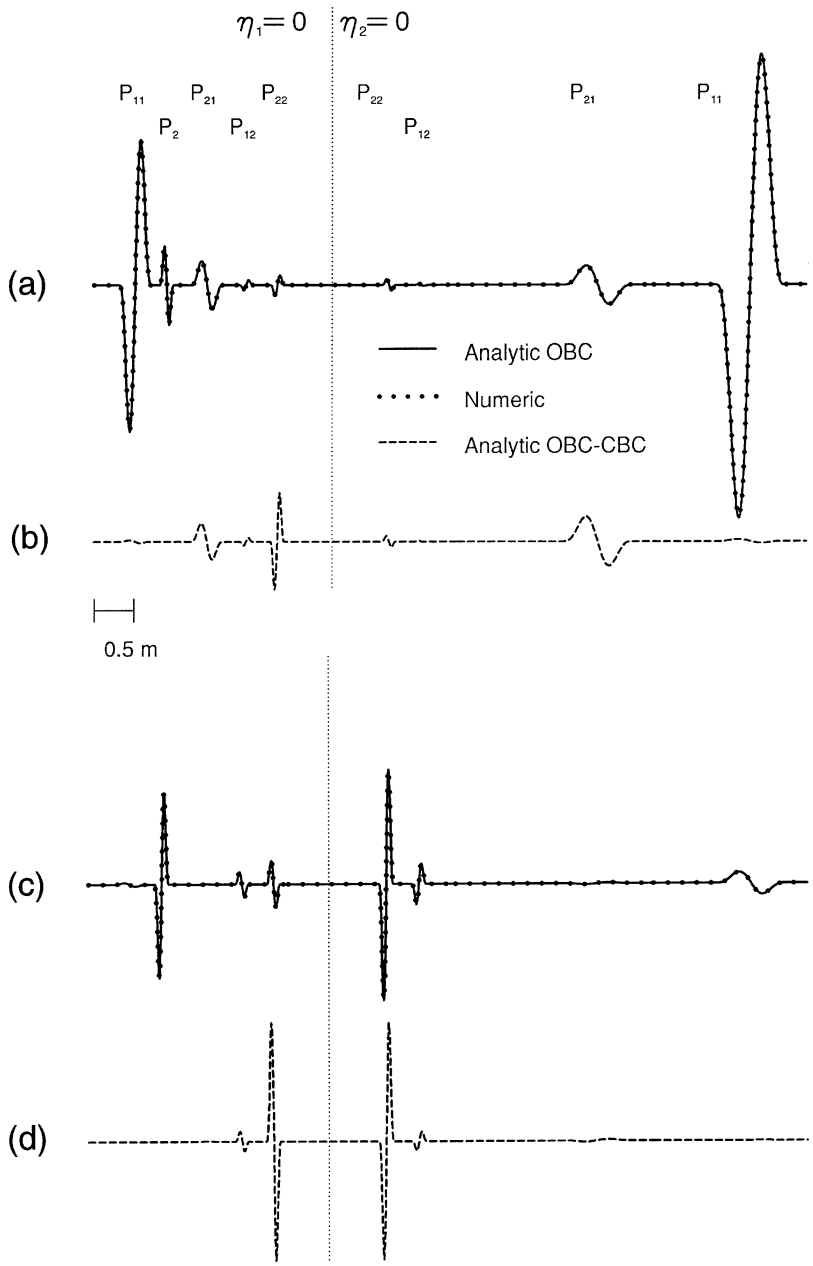

Figure 1. Theoretical and numerical snapshots of the non-dissipative acoustic field for v (a) and q (c). P_{ij} stands for wave type, $i, j = 1, 2$, fast and slow, respectively. The first subindex indicates the type of incident wave and the second the type of scattered wave. The source is in the left medium. P_2 corresponds to the direct slow wave travelling to the left. OBC and CBC denote open and closed boundary conditions, respectively. The snapshots (b) and (d), corresponding to v and q respectively, represent the difference between the OBC and the CBC theoretical responses. The analytical reflection coefficients R_{11} (e) and R_{12} (f) as a function of the surface impedance k.

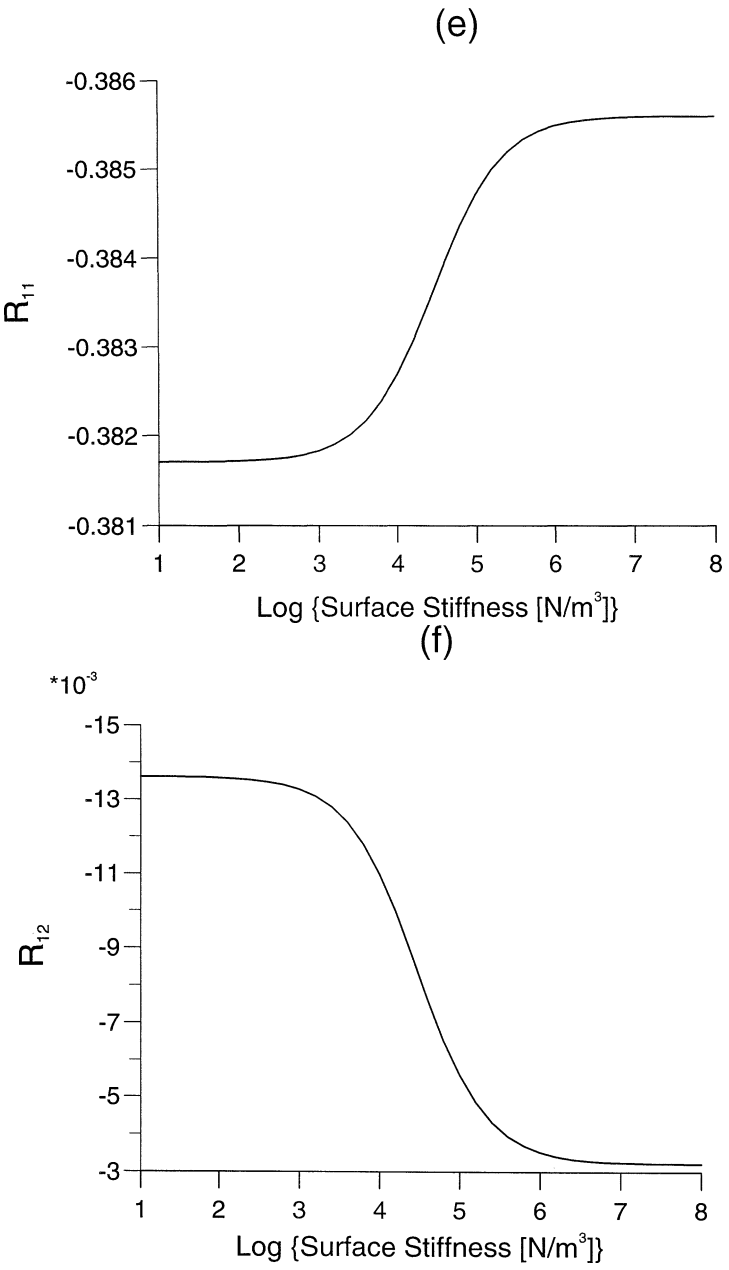

Figure 1. (Continued)

this case, the hydraulic conditions of the interface have changed and although the surface impedance has increased to 354 N/m^3, thus producing a MBC, the interfacial flow almost remains as if it were unrestrained (OBC) so that the difference in the magnitude of the scattered waves (MBC with $k = 354$ N/m^3 and OBC with $k = 0$)

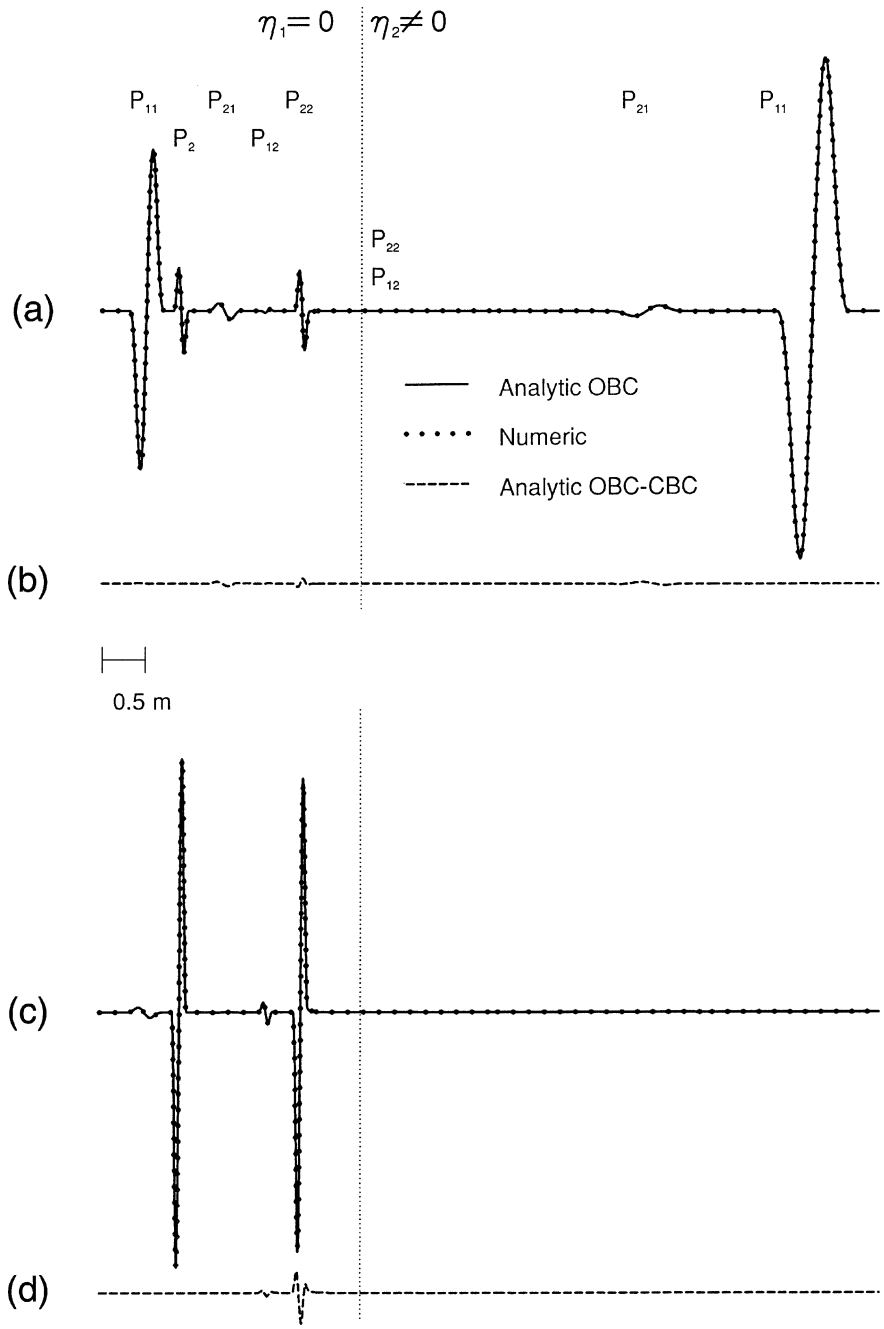

Figure 2. Theoretical and numerical snapshots of the acoustic field for v (a and b) and q (c and d). Plots (b) and (d) were obtained by subtracting the analytical response for an OBC from that for a CBC, as was done in plots 1b and 1d. In the transmission medium (right), the converted energy (P_{12} and P_{22}) is diffused near the interface. In (e), the amplitudes of the snapshots of q in a small zone near the interface have been enlarged.

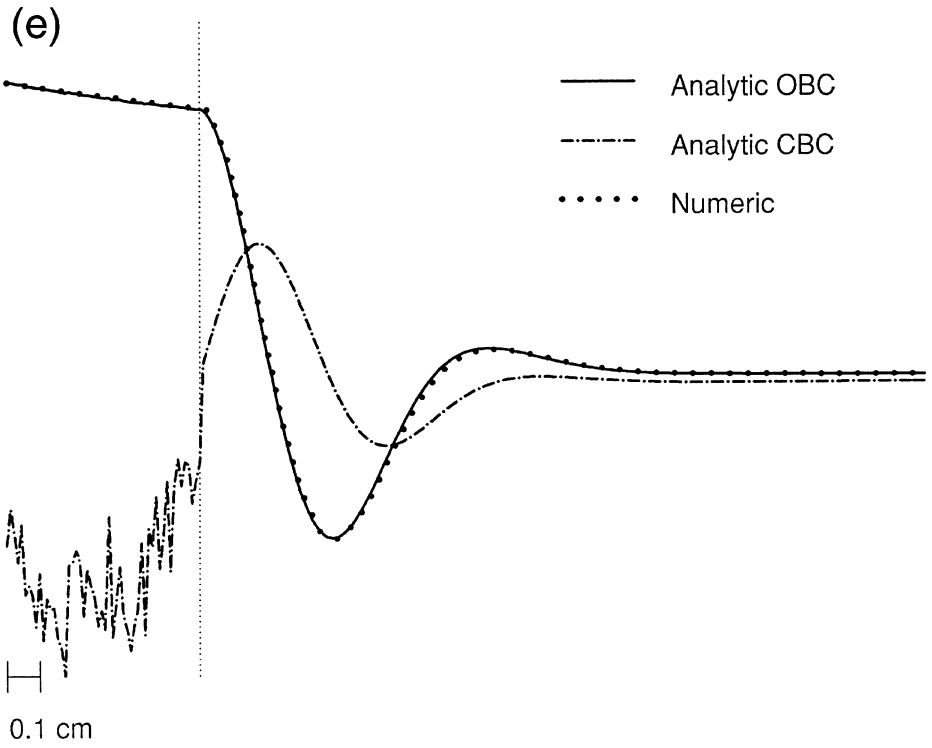

Figure 2. (Continued)

is unimportant. The amplitudes of the solid particle velocity v are twice as large as those of q, the filtration velocity. As opposed to the non-dissipative model, there is no significant difference between the seismic responses for an OBC and a CBC (figures 2b and 2d). The converted fast waves P_{21} are still sensitive to the type of boundary condition (figure 2b), but only in v as in the previous case.

Since the transmission medium is dissipative, static modes P_{12} and P_{22} have developed at the interface (not visible in these plots). They are the result of the slow waves becoming diffusive for the frequency range under consideration. The slow incident wave has produced a converted fast wave upon transmission P_{21}. An enlargement of the transmitted amplitudes corresponding to the relative fluid particle velocity (figure 2c) would also show an agreement between the analytical, obtained with an OBC, and the numerical solutions.

In order to determine the static mode behaviour at the interface as a function of the hydraulic conditions, we show in figure 2e a small zone about the interface with the amplitudes of q for the OBC case, enlarged approximately three orders of magnitude with respect to those of figure 2c. Since the scattered amplitudes in the CBC case (for $k = 10^7$ N/m^3) are smaller than those produced by the OBC, qualitatively in agreement with the experimental results of [16], they have been scaled up in addition, by a factor of 7 as compared to the OBC case. These snapshots were taken such that the slow

incident wave had not yet arrived. Therefore, the only converted energy corresponds to P_{12} (static mode) in the transmission medium and a slow reflected wave (P_{12} out of the range displayed). As can be seen in this figure, the numerical snapshot matches the analytical one for an OBC, although the surface impedance used to calculate the theoretical waveforms was 354 N/m^3, which corresponds to MBC. This is confirmed in the plot where it shows a finite value of the filtration velocity. On the other hand, fluid flow in the CBC (theoretical) case is not produced at the interface, as confirmed by this figure (dash-dotted line). The zero base line falls approximately where the amplitudes reach constant values at the right end of the snapshot.

The last example resembles a lab experiment [15] in which a plane wave from a water layer impinged on a porous sample. By measuring the ratio of the fluid pressure drop at the boundary and the filtration velocity in the water-saturated porous sample, it was found to reproduce the OBC case. The analogy with our example is that the water superstrate can be visualized as a porous layer in the limit case when $\kappa \to \infty$, so that the pore fluid mobility is infinitely large.

In the case presented in figure 3, both media are permeated with viscous fluids and therefore, the converted energy from the incident fast wave is diffused near both sides of the interface. An amplitude enlargement about the source location would also show the static modes which resulted from the direct slow waves becoming diffusive in this frequency range [4,5].

As far as the fast scattered waves are concerned, the two boundary conditions, OBC and CBC produce nearly the same amplitudes (a difference of the order of 10^{-5}), as can be seen in figure 3b. This small amplitude difference is counterbalanced by a difference in the amplitudes of static modes surrounding the interface. A closer look at the interface of the filtration velocity q, shown in figure 3c, shows that the numerical modelling produces practically a CBC. This result may appear surprising since both media have high porosities, which may imply a high pore interconnectivity. However, the hydraulic permeability in the incidence medium is very small, restraining effectively the amount of flow. In figure 3c, the amplitudes of the OBC snapshot have been reduced approximately by a factor of 13 in order to compare the shapes with those obtained by considering the CBC case. The surface impedance k estimated from the numerical modelling was slightly less than 10^7, in agreement with results published in the literature for the case of a CBC [15]. This value was then input for the analytical calculation of the waveforms and as can be observed in figure 3b, it agrees with the results obtained with the numerical modelling.

It should be noted that the OBC snapshot is composed of two static modes joined together at the interface, producing a continuous particle velocity field. They are the result of the fast wave energy conversion upon reflection (with the polarity reversed) and upon transmission, respectively. The shape of the theoretical OBC snapshot resembles the time-derivative of the source wavelet with its maximum located at the interface, although the left-half is not perfectly symmetrical with respect to the right-half. This effect is due to the smaller wavelength of the static mode in the incidence medium, because of lower phase velocity, than the one in the transmission

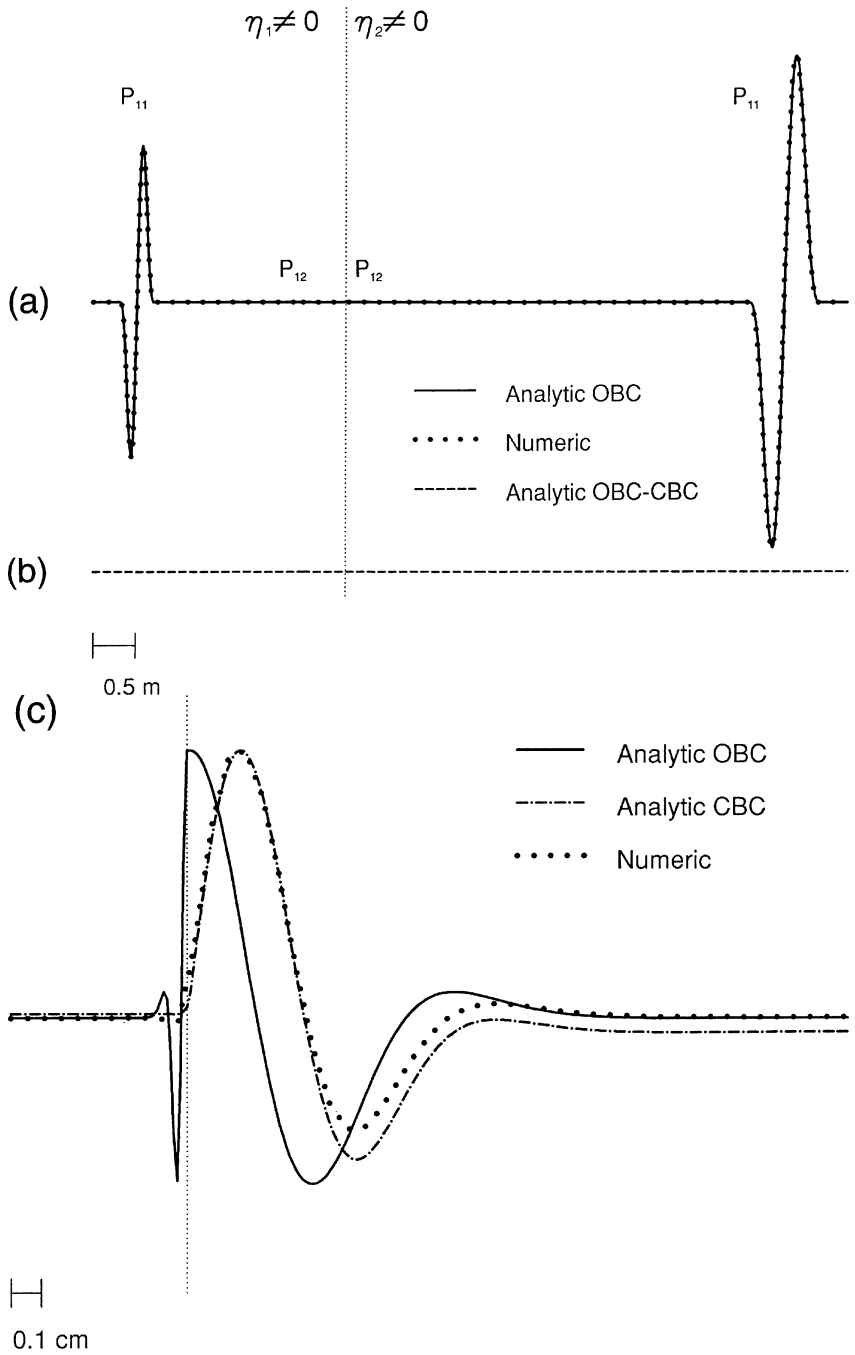

Figure 3. Theoretical and numerical snapshots of the dissipated acoustic field for v (a). Plot (b) is the snapshot obtained by subtracting the OBC and OBC theoretical responses. Plot (c) corresponds to q in a small zone surrounding the interface with the amplitudes enlarged approximately five orders of magnitude.

medium. The CBC snapshot resembles the 2D transient response of a cylindrical source in a single-phase viscoelastic medium.

6. Summary and conclusions

The purpose of this study was to determine the heterogeneous modelling behaviour at an interface between two porous media within the frame of Biot's theory, assuming the boundary conditions of [8]. The only difficulty in the analysis of the theoretical waveforms was the dependency of the formulation of the boundary conditions on the surface impedance k. However, these values for the surface stiffness were estimated directly from the results obtained with the numerical modelling, simply by computing the ratio of the calculated pore fluid pressure drop from the two nodes adjacent to the interface and the filtration velocity near the boundary.

The effect of modifying the pore fluid mobilities in both media, while keeping the porosites high but dissimilar, was to change the interface hydraulic conditions. This allowed us to carry out an investigation of the OBC, MBC and CBC cases. When the model media are permeated with inviscid fluids, the numerical and analytical results produce an OBC. If the transmission medium is saturated with a viscous fluid, the numerical modelling and the theoretical waveforms produce a MBC, although for practical purposes, the value of the surface impedance is very small such that MBC and OBC are practically the same. When the model is fully dissipative, i.e., permeated with fluids having finite viscosity, both the numerical and analytical reproduce a MBC, although the value of the surface stiffness is so high that it is practically the same as in the CBC case. Therefore, it is found that the heterogeneous modelling represents correctly the wave diffusion and propagation phenomena attendant at the boundary.

Acknowledgements

The authors wish to thank the reviewers for their suggestions to improve the paper. This work was funded in part by the European Commission in the framework of the JOULE programme, sub-programme Advanced Fuel Technologies.

Appendix A: Green's function in a homogeneous medium

The frequency-domain Green's function for a 2D homogeneous medium was obtained in Carcione and Quiroga-Goode [5]. The 1D solution is a particular case and is, for $x > -x_0$, given by

$$v = \psi_1 \exp\left[\mathrm{i}\omega(x + x_0)/V_1\right] + \psi_2 \exp\left[\mathrm{i}\omega(x + x_0)/V_2\right] \tag{15}$$

and

$$q = \chi_1 \exp\left[\mathrm{i}\omega(x + x_0)/V_1\right] + \chi_2 \exp\left[\mathrm{i}\omega(x + x_0)/V_2\right], \tag{16}$$

where ω is the angular frequency, and

$$V_{1(2)}^2 = \frac{2 \det \boldsymbol{M}}{U \pm (U^2 - 4 \det \boldsymbol{M} \det \boldsymbol{B}^{-1})^{1/2}}, \tag{17}$$
$$U = 2\rho_f C - \rho M - H\left(m - \frac{\mathrm{i}}{\omega}\frac{\eta}{\kappa}\right)$$

define the complex velocities V_1 and V_2 of the fast ($+$ sign) and slow ($-$ sign) compressional waves. In equation (17),

$$\boldsymbol{M} = \begin{bmatrix} -H & C \\ -C & M \end{bmatrix}. \tag{18}$$

Moreover,

$$\psi_1 = \frac{(V_1 V_2)^2}{V_2^2 - V_1^2}\left[\left(d_{11} - V_2^{-2}\right)s_1' + d_{12}s_2'\right], \tag{19}$$
$$\psi_2 = s_1' - \psi_1, \tag{20}$$
$$\chi_1 = -\frac{(V_1 V_2)^2}{V_2^2 - V_1^2}\left[\left(d_{22} - V_2^{-2}\right)s_2' + d_{21}s_1'\right], \tag{21}$$
$$\chi_2 = s_2' - \chi_1, \tag{22}$$

where

$$\boldsymbol{D} \equiv \begin{bmatrix} d_{11} & d_{12} \\ d_{21} & d_{22} \end{bmatrix} = (\boldsymbol{BM})^{-1} \tag{23}$$

and

$$\boldsymbol{S}' = \left[s_1', s_2'\right]^T = -\frac{\mathrm{i}\omega}{2}\boldsymbol{M}^{-1}\boldsymbol{S}. \tag{24}$$

Appendix B: Reflection and transmission coefficients

Let us consider two 1D inviscid ($\eta = 0$) porous media in contact at $x = 0$, and assume that a fast compressional wave, generated at $x = -x_0$, impinges upon an interface. In the incidence medium, the incident and reflected fields are

$$v_I = \exp\left[\mathrm{i}\omega(x + x_0)/V_1\right], \tag{25}$$
$$q_I = \beta_1 \exp\left[\mathrm{i}\omega(x + x_0)/V_1\right], \tag{26}$$

and

$$v_R = R_{11}\exp(-\mathrm{i}\omega x/V_1) + R_{12}\exp(-\mathrm{i}\omega x/V_2), \tag{27}$$
$$q_R = \beta_1 R_{11}\exp(-\mathrm{i}\omega x/V_1) + \beta_2 R_{12}\exp(-\mathrm{i}\omega x/V_2), \tag{28}$$

with

$$\beta_1 \equiv \frac{\chi_1}{\psi_1} = \frac{V_2^{-2} - d_{22}}{d_{12}}, \qquad \beta_2 \equiv \frac{\chi_2}{\psi_2} = \frac{V_1^{-2} - d_{22}}{d_{12}}, \tag{29}$$

where the characteristic equation $(d_{11} - V_i^2)(d_{22} - V_i^2) - d_{12}d_{21} = 0,\ i = 1, 2$, has been used. The transmitted field is

$$v' = T_{11} \exp\left(\mathrm{i}\omega x/V_1'\right) + T_{12} \exp\left(\mathrm{i}\omega x/V_2'\right), \tag{30}$$

$$q' = \beta_1' T_{11} \exp\left(\mathrm{i}\omega x/V_1'\right) + \beta_2' T_{12} \exp\left(\mathrm{i}\omega x/V_2'\right), \tag{31}$$

where R_{11} and R_{12} are the reflection coefficients of the fast and slow waves in the solid phase, and T_{11} and T_{12} are the corresponding transmission coefficients. The first subindex indicates the type of incident wave and the second denotes the scattered wave. The primed quantities correspond to those in the transmission medium. For simplicity, the factor $\exp(-\mathrm{i}\omega t)$ has been omitted in equations (25)–(31).

The boundary conditions (at x = 0) were given by Deresiewicz and Skalak [8]. They are

$$v = v', \qquad q = q', \qquad p = p', \qquad p_f - p_f' = kq, \tag{32}$$

where k is the coefficient of resistance, also called surface flow impedance [17]. The inverse of k has the dimension of hydraulic permeability per unit length [2]. Equations (32) model the different types of boundary conditions through the parameter k:

- $k = 0$ implies OBC (open interface).
- $k = \infty$ implies CBC (sealed interface). In this case, the last equation in (32) is replaced by $q = 0$.
- $0 < k < \infty$ implies MBC (partially open interface).

Substituting equations (25)–(31) into the OBC and MBC boundary conditions gives

$$\begin{bmatrix} 1 & 1 & -1 & -1 \\ \beta_1 & \beta_2 & -\beta_1' & -\beta_2' \\ a_1 & a_2 & a_1' & a_2' \\ b_1 & b_2 & b_1' - \beta_1' k & b_2' - \beta_2' k \end{bmatrix} \begin{bmatrix} R_{11} \\ R_{12} \\ T_{11} \\ T_{12} \end{bmatrix} = \begin{bmatrix} -1 \\ -\beta_1 \\ a_1 \\ b_1 \end{bmatrix} \exp(\mathrm{i}\omega x_0/V_1). \tag{33}$$

Similarly, CBC implies

$$\begin{bmatrix} 1 & 1 & -1 & -1 \\ \beta_1 & \beta_2 & -\beta_1' & -\beta_2' \\ a_1 & a_2 & a_1' & a_2' \\ 0 & 0 & \beta_1' & \beta_2' \end{bmatrix} \begin{bmatrix} R_{11} \\ R_{12} \\ T_{11} \\ T_{12} \end{bmatrix} = \begin{bmatrix} -1 \\ -\beta_1 \\ a_1 \\ 0 \end{bmatrix} \exp(\mathrm{i}\omega x_0/V_1). \tag{34}$$

Repeating the calculation for a slow compressional incident wave, we obtain for OBC and MBC:

$$\begin{bmatrix} 1 & 1 & -1 & -1 \\ \beta_1 & \beta_2 & -\beta_1' & -\beta_2' \\ a_1 & a_2 & a_1' & a_2' \\ b_1 & b_2 & b_1' - \beta_1' k & b_2' - \beta_2' k \end{bmatrix} \begin{bmatrix} R_{21} \\ R_{22} \\ T_{21} \\ T_{22} \end{bmatrix} = \gamma_s \begin{bmatrix} -1 \\ -\beta_2 \\ V_2^{-1} a_2 \\ V_2^{-1} b_2 \end{bmatrix} \exp(\mathrm{i}\omega x_0/V_2). \tag{35}$$

Similarly, CBC implies

$$\begin{bmatrix} 1 & 1 & -1 & -1 \\ \beta_1 & \beta_2 & -\beta_1' & -\beta_2' \\ a_1 & a_2 & a_1' & a_2' \\ 0 & 0 & \beta_1' & \beta_2' \end{bmatrix} \begin{bmatrix} R_{21} \\ R_{22} \\ T_{21} \\ T_{22} \end{bmatrix} = \gamma_s \begin{bmatrix} -1 \\ -\beta_2 \\ V_2^{-1} a_2 \\ 0 \end{bmatrix} \exp(\mathrm{i}\omega x_0/V_2), \tag{36}$$

where

$$a_r = -(H + C\beta_r)/V_r, \quad b_r = -(C + M\beta_r)/V_r, \quad r = 1, 2, \tag{37}$$

and

$$\gamma_s = \frac{\psi_2}{\psi_1}. \tag{38}$$

For $\eta \neq 0$ we get the reflection and transmission coefficients by applying the correspondence principle. It can be shown that the solution can be obtained by substituting $V_r(\eta = 0)$ with $V_r(\eta \neq 0)$, where V_r, $r = 1, 2$, is given in equation (17).

References

[1] M.A. Biot, J. Appl. Phys. 33 (1962) 1482–1498.
[2] T. Bourbie, O. Coussy and B. Zinszner, *Acoustics of Porous Media* (Institut Français du Petrole Publ., Paris, 1987).
[3] C. Boutin, G. Bonnet and P.Y. Bard, Geophys. J. R. Astr. Soc. 90 (1987) 521–550.
[4] J.M. Carcione and G. Quiroga-Goode, J. Comput. Acoust. 3 (1995) 261–280.
[5] J.M. Carcione and G. Quiroga-Goode, Geophysical Prospecting 44 (1996) 99–129.
[6] N. Dai, A. Vafidis and E.R. Kanasewich, Geophysics 60 (1995) 327–340.
[7] H. Deresiewicz and A. Levy, Bull. Seism. Soc. Am. 57 (1967) 381–391
[8] H. Deresiewicz and R. Skalak, Bull. Seism. Soc. Am. 53 (1963) 783–788.
[9] J. Geertsma and D.C. Smit, Geophysics 26 (1961) 169–181.
[10] M.K. Jain, *Numerical Solutions of Differential Equations* (Wiley Eastern Ltd., 1984).
[11] K.R. Kelly, R.W. Ward, S. Treitel and R.M. Alford, Geophysics 41 (1976) 701–714.
[12] M. Korn and H. Stockl, J. Geophysics 50 (1982) 171–176.
[13] D. Kosloff, M. Reshef and D. Loewenthal, Bull. Seis. Soc. Am. 74 (1984) 875–891.
[14] P. Mora, Geophysics 52 (1987) 1211–1228.
[15] P.B. Nagy and G. Blaho, J. Acoust. Soc. Am. 95 (1994) 828–835.
[16] P.N.J. Rasolofosaon, Appl. Phys. Lett. 52 (1988) 780–782.
[17] J.H. Rosenbaum, Geophysics 39 (1974) 14–32.
[18] P. Samec and J.P. Blangy, Geophysics 57 (1992) 441–450.
[19] A. Turgut and T. Yamamoto, Geophysics 53 (1988) 1056–1067.
[20] X. Zhu and G. McMechan, Geophysics 56 (1991) 328–339.